

國立交通大學
電子物理學系
碩士學位論文

第二型能帶結構碲化錳鋅/碲碲化鋅
多重量子井之光學特性研究

Optical characteristics of type-II

$\text{Zn}_{0.97}\text{Mn}_{0.03}\text{Se}/\text{ZnSe}_{1-x}\text{Te}_x$ multiple quantum wells

研究生：邱鏡學

指導教授：周武清 教授

中華民國九十七年六月

第二型能帶結構碲化錳鋅/碲碲化鋅多重量子井之光學特性研究

Optical characteristics of type-II $\text{Zn}_{0.97}\text{Mn}_{0.03}\text{Se}/\text{ZnSe}_{1-x}\text{Te}_x$ multiple quantum wells

研究生：邱鏡學

Student : Ching-hsueh Chiu

指導教授：周武清 教授

Advisor : Prof. Wu-ching Chou

國立交通大學



A Thesis

Submitted to Institute of Electrophysics

College of Science

National Chiao Tung University

In partial Fulfillment of the Requirements

For the Degree of Master

in

Electrophysics

April 2008

Hsinchu, Taiwan, Republic of China

中華民國九十七年六月

第二型能帶結構碲化鋅/碲化鋅多重量子井之光學特性研究

研究生：邱鏡學

指導教授：周武清 博士

國立交通大學電子物理學系

中文摘要

利用光激螢光量測技術來分析碲化鋅/碲化鋅(碲含量佔 8 和 20 莫耳百分比)多重量子井之光學特性。此多重量子井是以分子束磊晶系統所成長，碲化鋅層井寬分別為 2、3 和 5 奈米。隨著雷射功率強度的增加，量測到光激螢光光譜峰值有明顯的藍位移，這是能帶彎曲效應所造成，由此可以驗證此多重量子井是第二型能帶結構。由光激螢光變溫光譜實驗，可求得樣品的活化能。我們也利用時間解析光譜實驗分析載子的複合機制，發現載子的生命期會隨著不同的碲含量以及碲化鋅厚度而改變，這是因為電子與電洞的波函數重疊情形受到了改變。時間解析光譜隨雷射功率強度而呈現的非單一指數曲線，也可以用能帶彎曲模型解釋。

Optical characteristics of Type-II

$\text{Zn}_{0.97}\text{Mn}_{0.03}\text{Se}/\text{ZnSe}_{1-x}\text{Te}_x$ Multiple quantum wells

Student : Ching-hsueh Chiu

Advisor : Dr. Wu-Ching Chou

**Institute of Electrophysics
National Chiao Tung University**

Abstract

The $\text{Zn}_{0.97}\text{Mn}_{0.03}\text{Se}/\text{ZnSe}_{1-x}\text{Te}_x$ ($x = 0.08$ and 0.20) multiple quantum wells (MQWs) grown by molecular beam epitaxy were studied by photoluminescence (PL) measurements. The $\text{ZnSe}_{1-x}\text{Te}_x$ well thickness varies among 2, 3, and, 5 nm. The PL peak energy shows a giant blue-shift with excitation power due to the band-bending effect. The activation energies of the MQWs were also obtained by temperature-dependent PL measurements. We also studied the mechanism of carrier recombination by the time-resolved photoluminescence (TRPL) experiments. The dependence of PL lifetimes on the Te concentration and well width can be explained by the variation of electron-hole wavefunction overlapping. Moreover, the non-single-exponential PL decays of the power-dependent TRPL measurements can be understood by the band-bending model.

Acknowledgement

在**交大電物所**兩年的研究生活即將進入尾聲，回想這段時間以來，有歡笑、有淚水、有高興、有失落，在這期間讓我學到不少東西及交到許多好朋友，比起大學時候的我更成長了不少。

首先謝謝**周武清**教授，在我這兩年研究生涯提供充足的研究資源，不厭其煩的教導，使我在研究和處理事情中都學到不少寶貴知識，讓再往研究之路邁進的我幫助很大；再來要感謝奈米科技實驗室學長姐的熱心指導我，感謝**彥丞、繼祖、謝博、瑞雯、怡仁、狗哥、瑞泰**，沒有你們辛苦的傳承實驗技術和方法，勢必我的研究之路不會這麼順遂；特別感謝彥丞學長在這段期間一起研究及討論，協助我解釋實驗數據並解決實驗困難，回想起來是我最甜美的時光，也以彥丞學長看齊，成為一位好學長；還要感謝實驗室伙伴**復凱**，在研究期間一起努力打拼，希望你能賺大錢去雲南找天仙妹妹；還有**威智、俊榮**兩位學弟，希望你們能和彥丞學長合作把高壓團隊壯大起來，也期許你們未來一年的研究工作順利完成；另外要感謝中原大學同學們，**奕男、政雄、政道、雅婷**，雖然大家都在各校研究所就讀，但是常常互相鼓勵對方，使我們友情常存不變質，尤其奕男，從大學時期一起努力學業，到研究所時期常見面互相鼓勵，是我快樂的泉源，希望能早日達成你的夢想。

最後，很感謝我的家人，有你們全力支持，讓我有用不完的動力，尤其**爸爸、媽媽**，有你們提供優渥的環境和精神鼓勵，使我常常創造新記錄和開創新局，也謝謝**妹妹**的鼓勵，希望你能早日實現夢想；我也期許自己：「**相信自己，我一定做的到！**」

Index

Abstract (Chinese version)	i
Abstract (English version)	ii
Acknowledgement	iii
Index	iv
Chapter 1 : Introduction	1
Chapter 2 : Experiments	3
2-1 Sample preparation	3
2-2 Photoluminescence (PL) system	5
2-3 Time-resolved photoluminescence (TRPL) system	6
Chapter 3 : Results and discussion	12
3-1 Emission properties of $Zn_{1-x}Mn_xSe/ZnSe_{1-y}Te_y$ MQWs	12
3-2 Dynamics of carrier recombination	15
Chapter 4 : Conclusions	30
References	31

Chapter 1 : Introduction

Wide-band-gap II-VI isoelectronic semiconductor, $\text{ZnSe}_{1-x}\text{Te}_x$, has attracted much attention due to their applications in blue/green light-emitter materials [1-2]. The optical properties of isoelectronic localized states have also been studied in the past decades, such as GaAsN [3], ZnSTe [4,5], and ZnSeTe [6-8]. Recently, $\text{ZnSe}_{1-x}\text{Te}_x$ alloys have been under extensive investigation. For example, Spectacular atomic ordering has been observed in $\text{ZnSe}_{0.5}\text{Te}_{0.5}$ specimens, which self-organize to form modulated $\text{ZnSe}_{1-x}\text{Te}_x$ superlattices [9]. In order to investigate the recombination dynamics of $\text{ZnSe}_{1-x}\text{Te}_x$ ternary compound semiconductor, the time-resolved photoluminescence (TRPL) technique was used. It was shown that the PL decay time of bulk ZnSe is about 200 ps [10] while it is about 30 ns for $\text{ZnSe}_{1-x}\text{Te}_x$ ($x = 0.12$) epilayer [11]. Due to the spatial separation of electrons and holes in a type-II quantum structure, the wavefunction overlap between electrons and holes is largely decreased. Therefore, the observed PL lifetime will be longer than that in a type-I structure. For example, the PL decay time for type-II ZnTe/ZnSe superlattice is about 100 ns [12].

In this thesis, the type-II $\text{Zn}_{0.97}\text{Mn}_{0.03}\text{Se}/\text{ZnSe}_{1-x}\text{Te}_x$ multiple quantum wells (MQWs) are studied by PL and TRPL. The PL decay time are expected to be longer than the normal type-II quantum structure because of the existence of Te isoelectronic center. In chapter 2, the sample preparations of molecular-beam epitaxy (MBE) are introduced. In

addition, the optical measurements are also introduced, including photoluminescence (PL) and TRPL. In chapter 3, the experimental results about power-dependent PL, temperature-dependent PL, and carrier recombination dynamics are discussed. Finally, a brief conclusion of current work is given in chapter 4.



Chapter 2 : Experiment

In this chapter, the sample growth of $\text{Zn}_{0.97}\text{Mn}_{0.03}\text{Se}/\text{ZnSe}_{1-x}\text{Te}_x$ MQWs and the experimental techniques used in this thesis are described. The experimental techniques include the conventional PL, power-dependent PL and TRPL.

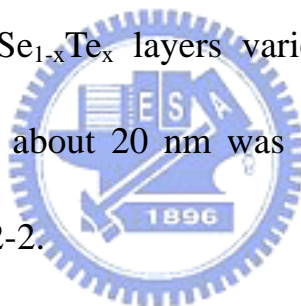
2.1 Sample preparation

The type-II $\text{Zn}_{0.97}\text{Mn}_{0.03}\text{Se}/\text{ZnSe}_{1-x}\text{Te}_x$ MQWs were grown on GaAs (001) substrates by Veeco Applied EPI 620 molecular-beam epitaxy (MBE) system. Low-temperature effusion cells were used for elemental Zn, Se, and Te sources. A standard effusion cell was used for Mn element. The growth conditions were listed in Table 2-1.

The schematic sample structure of $\text{Zn}_{0.97}\text{Mn}_{0.03}\text{Se}/\text{ZnSe}_{1-x}\text{Te}_x$ MQWs was shown in Fig. 2-1. The GaAs substrate was mounted on molybdenum disk holder by Indium. After the substrate holder was loaded on the transfer rod in the introduction chamber, the oil-free mechanical diaphragm pump and then the turbo pump were turned on. When the pressure of introduction chamber is below 10^{-8} torr, the manual gate valve was opened and the substrate holder (molybdenum disk) was transferred to the growth chamber by the substrate transfer arm. The substrate temperature was raised up to $650\text{ }^{\circ}\text{C}$ for removing the oxide on the GaAs substrate. The deposition procedure was monitored by the reflection high energy electron diffraction (RHEED). When clear RHEED pattern was

observed, the substrate temperature was decreased to 300 °C for the deposition of ZnSe buffer layer.

In order to decrease the lattice mismatch between GaAs and ZnMnSe layers, a ZnSe buffer layer of about 200 nm was grown before the ten periods of $\text{Zn}_{0.97}\text{Mn}_{0.03}\text{Se}/\text{ZnSe}_{1-x}\text{Te}_x$ ($x = 0.08$ and 0.20) MQWs. The Mn and Te concentration were determined by energy-dispersive x-ray (EDX) measurement on the respective $\text{Zn}_{0.97}\text{Mn}_{0.03}\text{Se}$ and $\text{ZnSe}_{1-x}\text{Te}_x$ epilayers grown with the same parameters. For the $\text{Zn}_{0.97}\text{Mn}_{0.03}\text{Se}/\text{ZnSe}_{1-x}\text{Te}_x$ MQWs, the thickness of the $\text{Zn}_{0.97}\text{Mn}_{0.03}\text{Se}$ layers is fixed at 20 nm while the thickness of $\text{ZnSe}_{1-x}\text{Te}_x$ layers varies from 5, 3, to, 2 nm. Finally, a $\text{Zn}_{0.97}\text{Mn}_{0.03}\text{Se}$ capping layer of about 20 nm was grown on the $\text{ZnSe}_{1-x}\text{Te}_x$ layer. The sample list was shown in Table 2-2.



2.2 Photoluminescence (PL) system

The schematic setup of the photoluminescence system is shown in Fig. 2-2. The samples were loaded on the cold finger of a closed cycle cryostat. The temperature can be controlled between 10 and 325 K. The sample was excited by an He-Cd 325 nm laser. The incident laser beam was focused on the sample by a convex lens (L_1). The combination of a set of convex lenses (L_2 and L_3) guided the luminescence into the double-grating spectrometer. A SPEX 1403 double-grating spectrometer equipped with a thermoelectrically cooled photo-multiplier tube (R928, Hamamatsu) was used to analyze the PL spectra. The spectrometer was controlled by a computer, which was used to store and plot the collected data.



2.3 Time-resolved Photoluminescence (TRPL) system

The schematic setup of the Time-resolved photoluminescence system is shown in Fig. 2-3. The GaN pulsed laser (405 nm) with a pulse width of 50 ps and a repetition rate of 2.5 MHz was used as an excitation source. The laser light was focused on the sample by a convex lens (L_1). The combination (L_2 and L_3) lenses guided the luminescence into the double-grating spectrometer. The signal was dispersed by a 0.85 m double-grating spectrometer and detected by a high-speed photomultiplier tube. The signal was further analyzed by a computer plug-in time-correlated counting card. The overall temporal resolution of the time-resolved PL measurement is about 0.3 ns.



Table 2-1. Effusion cell temperature (°C) and substrate temperature (°C) for the growth of the $Zn_{0.97}Mn_{0.03}Se/ZnSe_{1-x}Te_x$ MQWs.

	ZnSe	$Zn_{0.97}Mn_{0.03}Se$	$ZnSe_{0.92}Te_{0.08}$	$ZnSe_{0.80}Te_{0.20}$
T (Zn)	300	290	290	290
T (Mn)	-	690	-	-
T (Se)	170	170	170	170
T (Te)	-	-	295	280
T (Substrate)	300	320	320	320



Table 2-2. Sample parameters of the type-II $\text{Zn}_{0.97}\text{Mn}_{0.03}\text{Se}/\text{ZnSe}_{1-x}\text{Te}_x$ multiple quantum wells.

Sample Code	ZnSe (buffer layer)	$\text{Zn}_{0.97}\text{Mn}_{0.03}\text{Se}$	$\text{ZnSe}_{0.80}\text{Te}_{0.20}$
Sample A	200nm	20nm	5nm
Sample B	200nm	20nm	3nm
Sample C	200nm	20nm	2nm
	ZnSe (buffer layer)	$\text{Zn}_{0.97}\text{Mn}_{0.03}\text{Se}$	$\text{ZnSe}_{0.92}\text{Te}_{0.08}$
Sample D	200nm	20nm	5nm



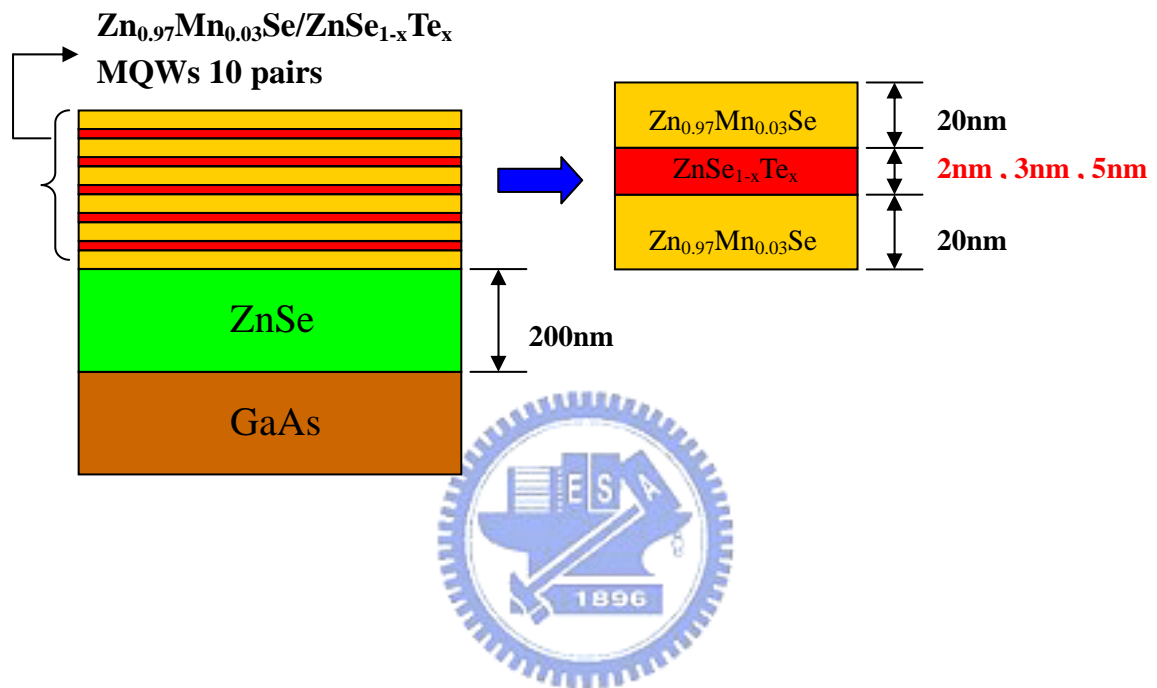


Fig. 2-1. Sample structure of $\text{Zn}_{0.97}\text{Mn}_{0.03}\text{Se}/\text{ZnSe}_{1-x}\text{Te}_x$ MQWs

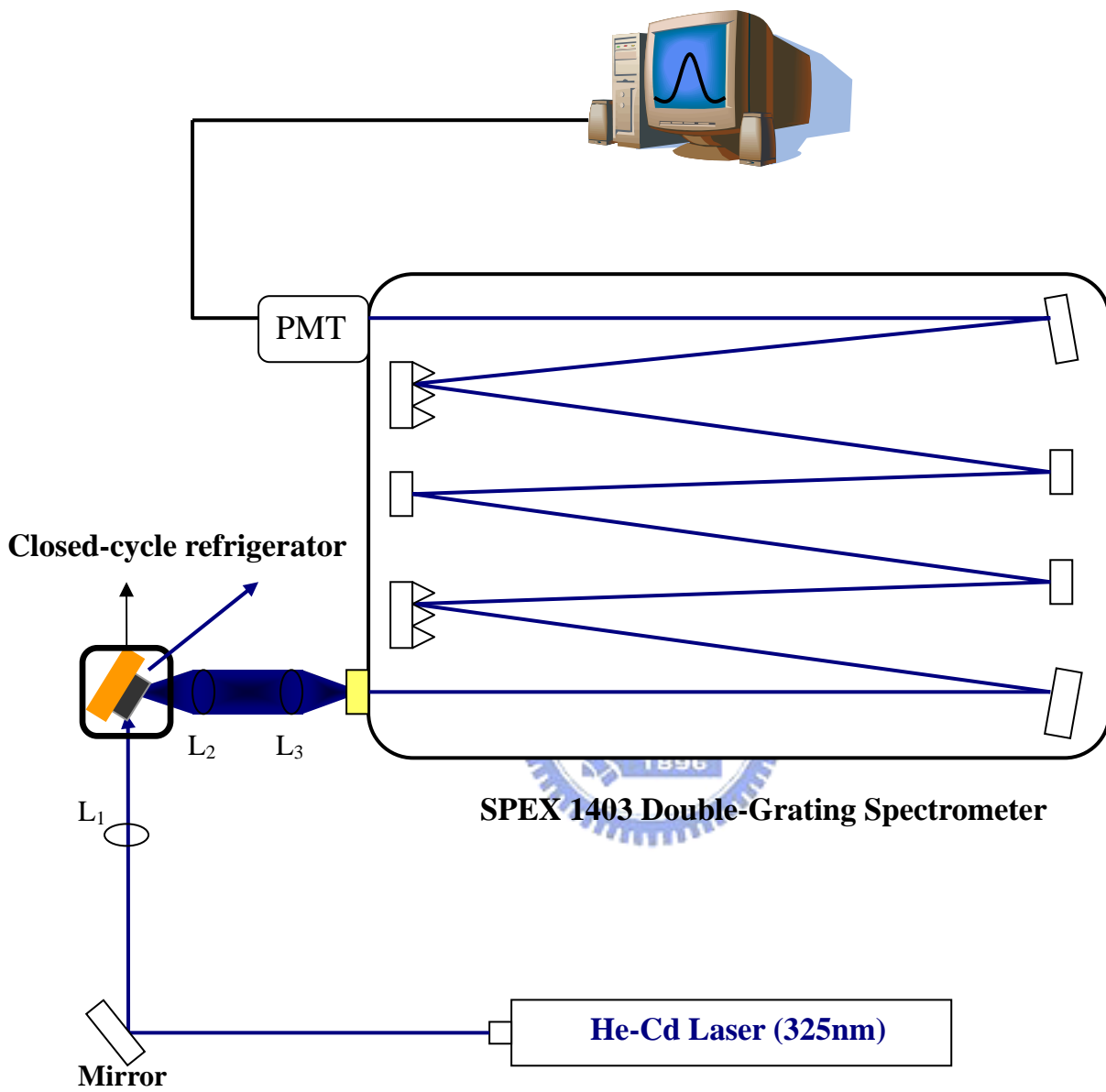


Fig. 2-2. The experimental setup of PL measurements.

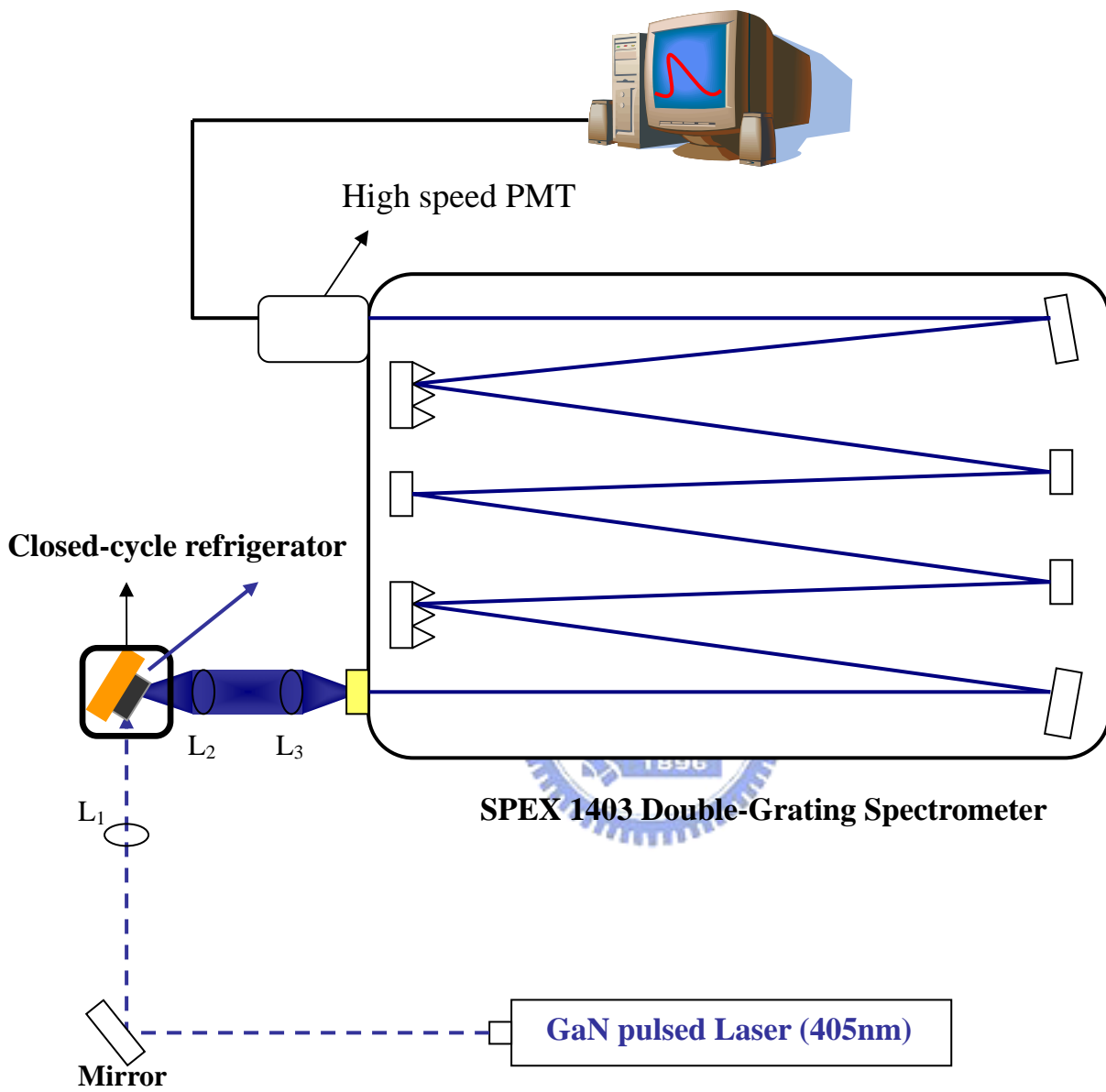


Fig. 2-3. The experimental setup of TRPL measurements.

Chapter 3 : Results and Discussion

In this chapter, we present the interesting optical characteristics of $\text{Zn}_{0.97}\text{Mn}_{0.03}\text{Se}/\text{ZnSe}_{1-x}\text{Te}_x$ ($x = 0.08$ and 0.20) MQWs measured by the conventional and time-resolved PL. The type-II band alignment of the $\text{Zn}_{0.97}\text{Mn}_{0.03}\text{Se}/\text{ZnSe}_{1-x}\text{Te}_x$ MQWs was verified by power-dependent PL measurement. The thermal activation energy (E_a) was determined from temperature-dependent PL spectra. The wavelength-dependent and temperature-dependent time-resolved PL measurements were used to study the carrier recombination processes and recombination kinetics of Te isoelectronic centers in the $\text{Zn}_{0.97}\text{Mn}_{0.03}\text{Se}/\text{ZnSe}_{1-x}\text{Te}_x$ MQWs system.



3.1 PL studies of $\text{Zn}_{0.97}\text{Mn}_{0.03}\text{Se}/\text{ZnSe}_{1-x}\text{Te}_x$ MQWs

Fig. 3-1 shows the PL spectra of $\text{Zn}_{0.97}\text{Mn}_{0.03}\text{Se}/\text{ZnSe}_{0.80}\text{Te}_{0.20}$ MQWs with different well thickness of $\text{ZnSe}_{0.80}\text{Te}_{0.20}$ layer at low temperature. All of the spectra consist of two emission bands. The sharp emission peak near 2.798 eV is attributed to the near band edge transition of $\text{Zn}_{0.97}\text{Mn}_{0.03}\text{Se}$ layer. The other emission, which is more sensitive to the well thickness, is due to the recombination in MQWs. A significant blue-shift about 200 meV was observed as the L_w decrease from 5 nm to 2 nm. This can be attributed to the quantum confinement effect. The broad PL peak exhibits asymmetry

line shape at low energy side. Due to holes are more strongly trapped by Te impurities at low energy. The broad PL line width is mainly due to inhomogeneous broadening caused by Te composition fluctuation that leads to asymmetrical PL curves. In addition the full width at half maximum (FWHM) of the PL curves increases with the decreasing of well thickness. This is due to the increasing well-width fluctuation [13-14].

The band alignment was determined by power-dependent PL. Fig. 3-2 (Fig.3-3) presents the results for the MQW of sample A (sample C). The PL peak has a blue-shift of about 48 meV (23 meV) when the pumping intensity changes from 0.1 mW to 45.0 mW. The peak position of PL spectra shows a significant blue-shift with the increasing excitation intensity. The inset shows the blue-shift of PL peak energy as a function of the cube of excitation power. The relationship is linear. This phenomenon is usually interpreted as the results of band-bending effect in type-II quantum structures [15-17]. The band-bending effect is caused by the spatially separated photo-excited carriers, in which electrons are confined in the ZnMnSe layers and holes are confined in the ZnSeTe layers. The electron-hole pairs are attracted through the Coulomb interaction. This leads to the bending of the valence and conduction band. The quantization energy was found to increase proportionally with the cube root of the excitation power. The type-II band alignment of $\text{Zn}_{0.97}\text{Mn}_{0.03}\text{Se}/\text{ZnSe}_{1-x}\text{Te}_x$ MQWs system was schematically shown in Fig. 3-4. The PL signal is generated from the recombination of the

accumulated holes trapped by Te isoelectronic impurities and electrons near the interface. The emission energy of the PL peak is smaller than the band gap of ZnMnSe and ZnSeTe.

The temperature-dependent PL spectra of sample A are shown in Fig. 3-5. The intensity gradually decreases as the temperature is increased from 13 to 300 K. Fig. 3-6 shows the variation of the integrated PL intensity as a function of the reciprocal temperature of sample A. The temperature-dependence of the integrated PL intensity (I_{PL}) could be expressed as

$$I(T) = \frac{I_0}{1 + A \exp\left(-\frac{E_a}{k_B T}\right)} \quad (1)$$

where I_0 is the integrated PL intensity at 0 K, T is the temperature, A is fitting constant, and $k_B = 8.62 \times 10^{-5}$ (eV · K⁻¹) is the Boltzmann constant. We have fitted our data using Eq. (1). The results of fitting are given in Table 3-1 and show that the E_a value is in the range of 60 - 46 meV for different quantum well thickness. Quenching of the luminescence with increasing temperature can be explained by thermal activation of carriers out of a confining potential [18-19].

3.2 TRPL studies of $\text{Zn}_{0.97}\text{Mn}_{0.03}\text{Se}/\text{ZnSe}_{1-x}\text{Te}_x$ MQWs

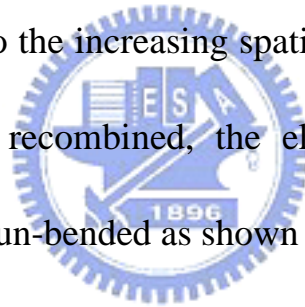
In order to understand the carrier recombination mechanism of the type-II MQWs, TRPL measurements are studied. Fig.3-7 displays the spectral distribution of τ_{PL} of the $\text{Zn}_{0.97}\text{Mn}_{0.03}\text{Se}/\text{ZnSe}_{1-x}\text{Te}_x$ MQWs ($x=0.08$ and 0.20). The decay time is composed of a faster initial component and a slower tail component. In order to resolve the time constant, all of the experimental data were fitted by a biexponential function described by

$$I(t) = I_1 \exp\left(\frac{-t}{\tau_1}\right)^\beta + I_2 \exp\left(\frac{-t}{\tau_2}\right) \quad (2)$$

where $I(t)$ is the PL intensity at time t , I_1 and I_2 are the relative intensity for τ_1 and τ_2 , respectively, β means the decay rate distribution. As shown in Fig. 3-7, the PL decay times decrease with the increasing detection energy. The samples of higher Te concentration exhibit longer PL decay times. Because when the Te concentration is increased, the holes are trapped by more Te-clusters, leading to less electron-hole wavefunction overlap. In addition, the τ_{PL} decreases with decreasing well thickness. It is due to the stronger electron-hole wavefunction overlap with the decreasing well width.

Fig. 3-8 (a) displays the PL spectrum of sample A at 13K. The PL decay times of sample A at various detection energies are shown in the Fig. 3-8 (b). The same behavior is also observed in other samples discussed herein. The PL decay curves are well-fitted

by equation (2). The decay time monotonically decreases with the increasing of detection energies. It is attributed to the stronger trapping of holes by the Te-clusters. It results in the suppression of electron-hole wavefunction overlap in low energy. Such a non-exponential decay is attributed to the band bending effect [20-21]. After the photoexcitation, a dipole layer is formed between the holes in the $\text{ZnSe}_{1-x}\text{Te}_x$ layer and electrons attracted in the surrounding $\text{Zn}_{0.97}\text{Mn}_{0.03}\text{Se}$. It builds up an electric field in type-II MQWs, which in turn gives rise to the bending of valence and conduction band. It further changes the overlapping of the electron and hole wave function. The faster initial decay time is attributed to the increasing spatial overlap due to the band-bending effect. After most of carriers recombined, the electron-hole wavefunction overlap decreases and the band become un-bended as shown in Fig. 3-9 (a) and (b).



To further support our investigations, we perform the power-dependent time-resolved PL measurements shown in Fig.3-10. The PL decay time is multi-exponential at high excitation intensities and it approaches a single exponential under lower excitation energy. The band bending effect depends strongly on the photo-excited carrier concentration. The initial fast decay time results from the higher carrier concentration caused by higher excitation intensity.

Fig. 3-11 shows the spectral distribution of PL decay time at different temperatures. The decay time monotonically decreases with the increasing of detection energies. The

sharp drop of decay times are much more pronounced at low temperature (13K). It is because the holes are strongly trapped by Te-clusters at 13 K. It leads to the decrease of electron-hole wavefunction overlap. At high temperature, the holes are less trapped by Te-clusters, then the electron-hole wavefunction overlap increases. Therefore, it manifests that the Te isoelectronic centers play an important role in the recombination dynamics of $\text{Zn}_{0.97}\text{Mn}_{0.03}\text{Se}/\text{ZnSe}_{1-x}\text{Te}_x$ MQWs.



Table 3-1. Activation energy of the $\text{Zn}_{0.97}\text{Mn}_{0.03}\text{Se}/\text{ZnSe}_{0.80}\text{Te}_{0.20}$ MQWs.

The $\text{ZnSe}_{0.80}\text{Te}_{0.20}$ thickness	E_a (meV)
5nm	60 ± 1
3nm	50 ± 1
2nm	46 ± 1



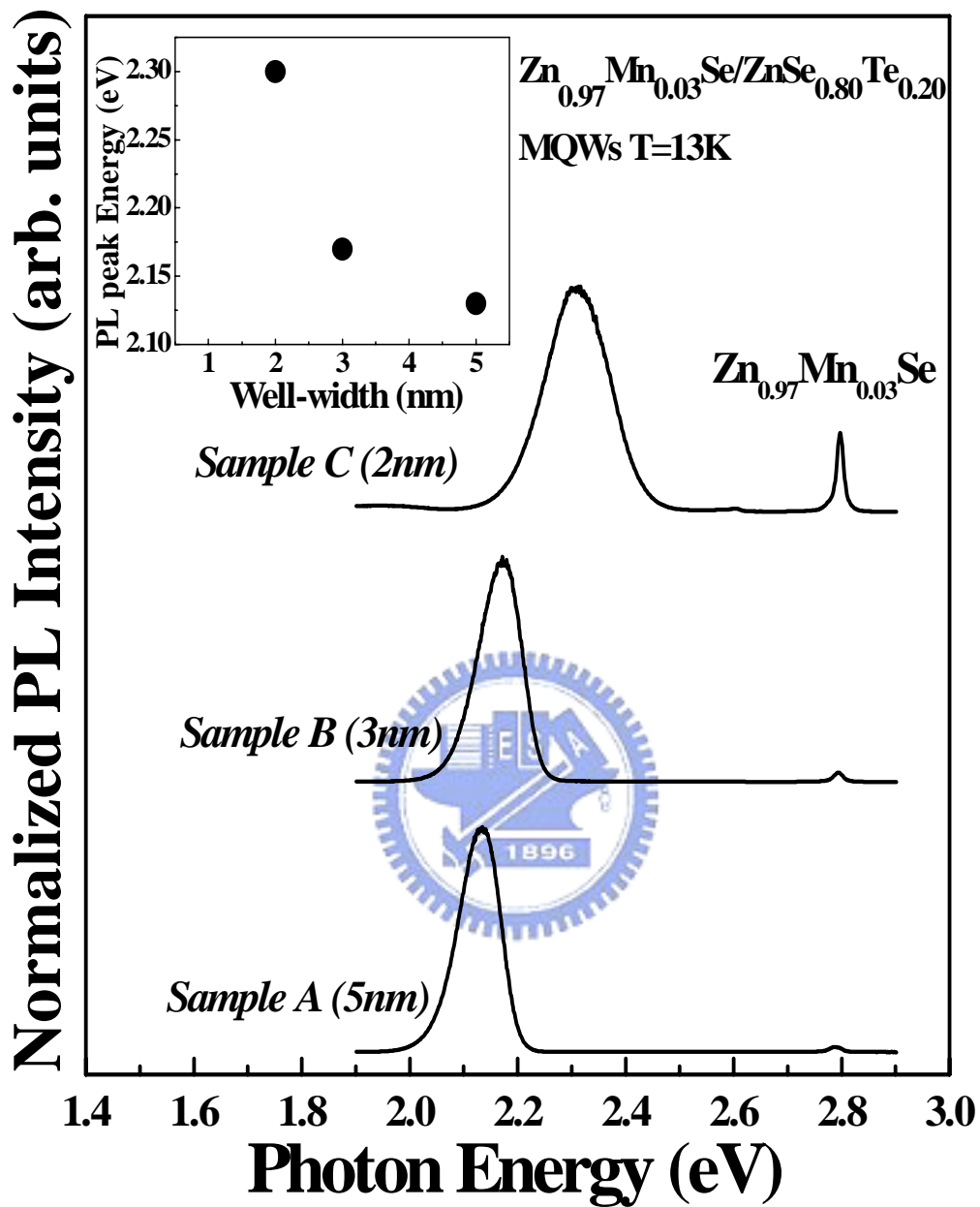


Fig. 3-1. Normalized PL spectra of $\text{Zn}_{0.97}\text{Mn}_{0.03}\text{Se}/\text{ZnSe}_{0.80}\text{Te}_{0.20}$ MQWs with different $\text{ZnSe}_{0.80}\text{Te}_{0.20}$ layer thickness at 13 K. The inset shows the measured PL peak energies as a function of the well width.

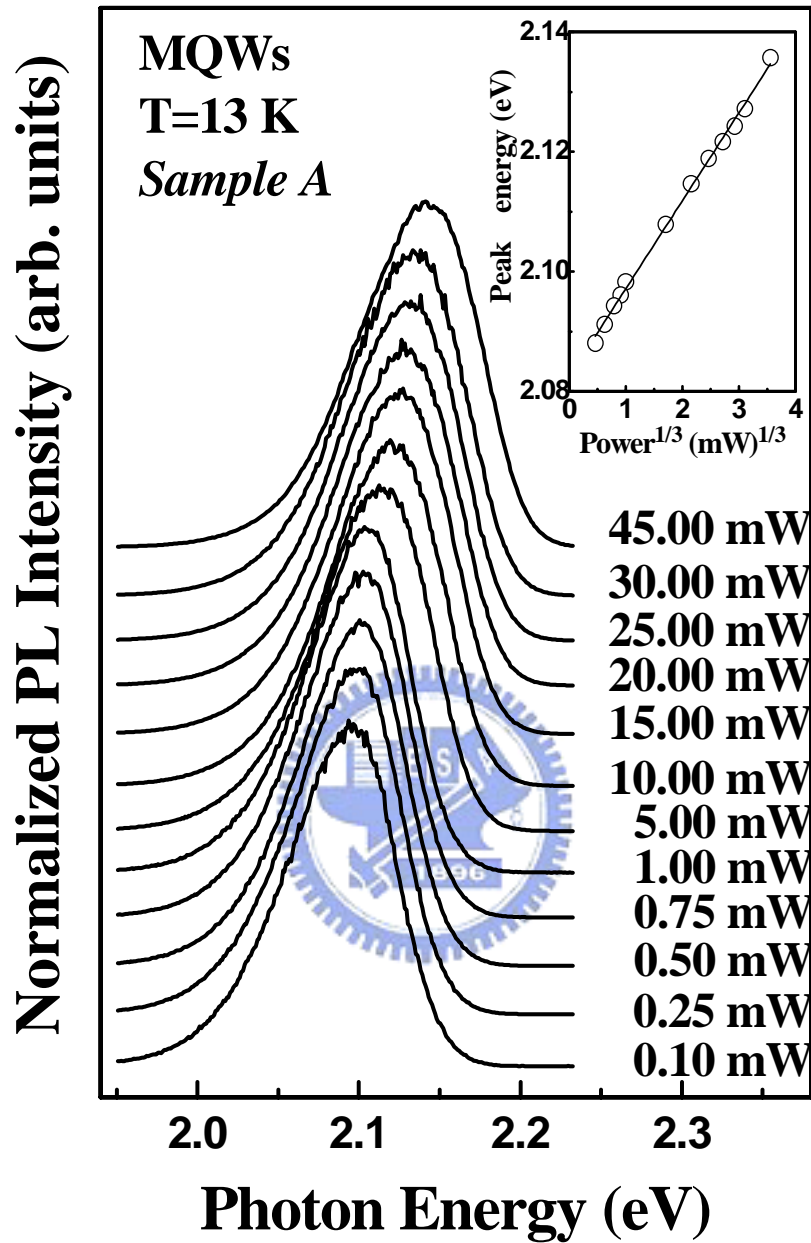


Fig. 3-2. PL spectra of $\text{Zn}_{0.97}\text{Mn}_{0.03}\text{Se}/\text{ZnSe}_{0.80}\text{Te}_{0.20}$ MQWs (sample A) under different excitation intensities at 13 K. The inset shows the measured PL energy (open circles) versus the cubic root of excitation power.

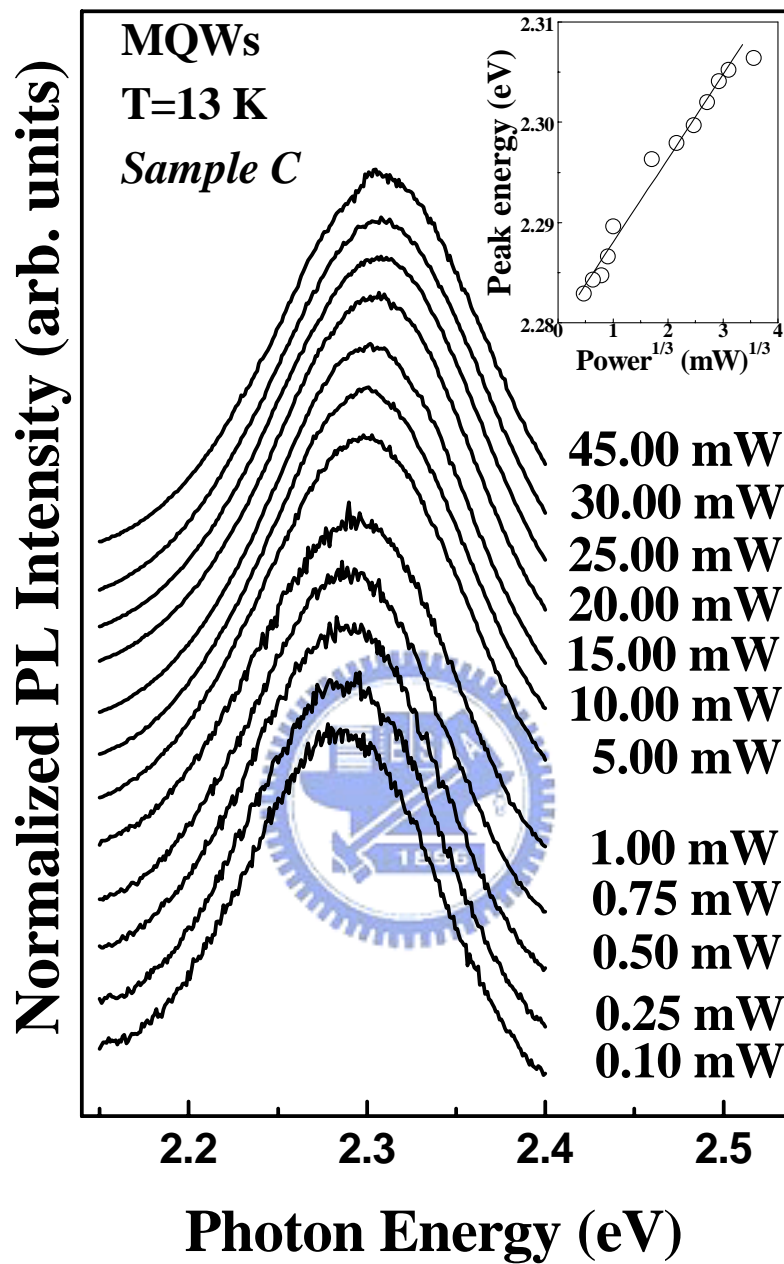


Fig. 3-3. PL spectra of $\text{Zn}_{0.97}\text{Mn}_{0.03}\text{Se}/\text{ZnSe}_{0.80}\text{Te}_{0.20}$ MQWs (sample C) under different excitation intensities at 13 K. The inset shows the measured PL energy (open circles) versus the cubic root of excitation power.

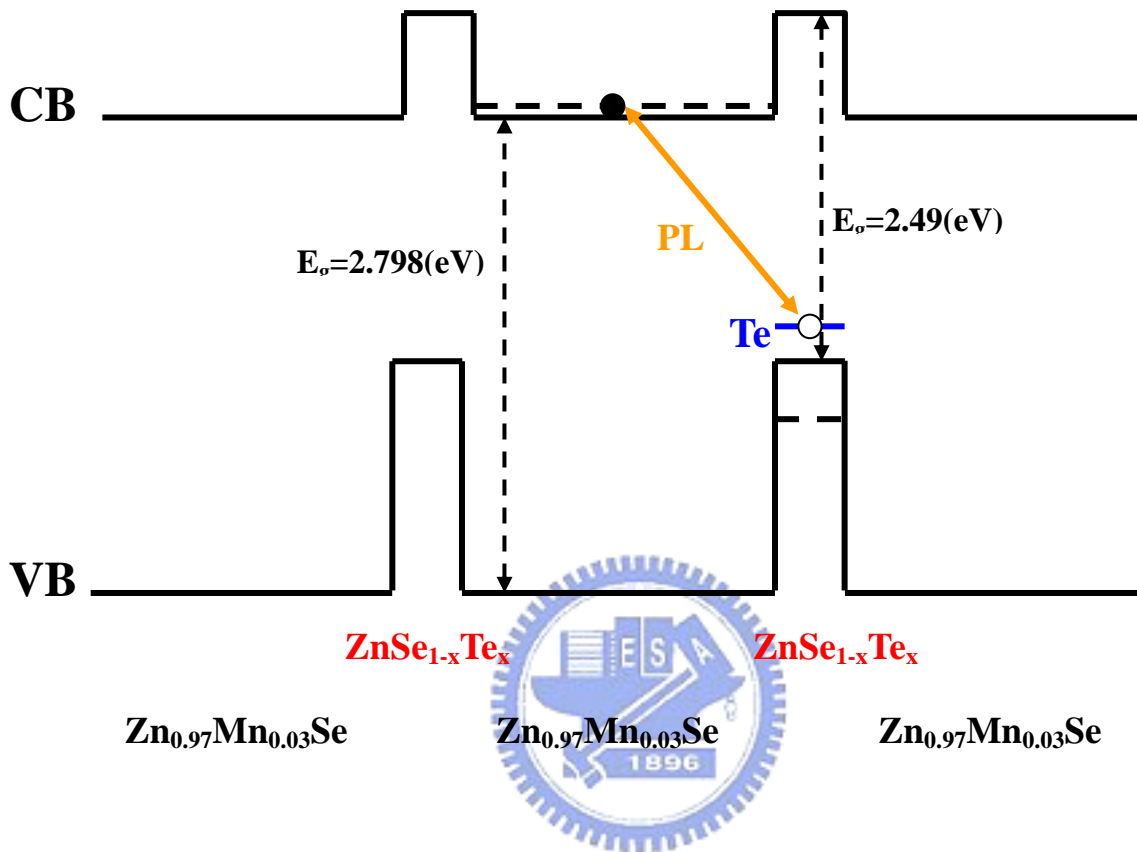


Fig. 3-4. Schematic diagram of type-II band alignment for $\text{Zn}_{0.97}\text{Mn}_{0.03}\text{Se}/\text{ZnSe}_{1-x}\text{Te}_x$ MQWs.

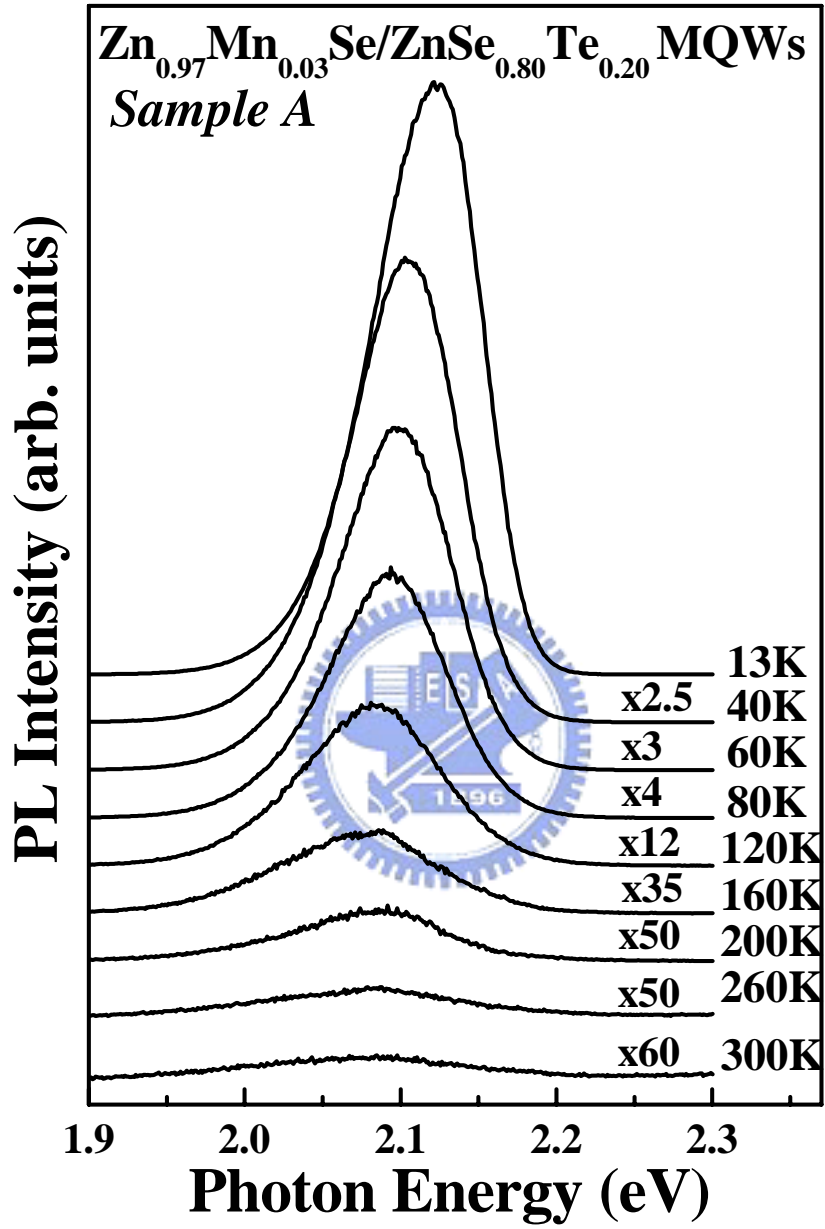


Fig. 3-5. Temperature-dependent PL spectra of sample A.

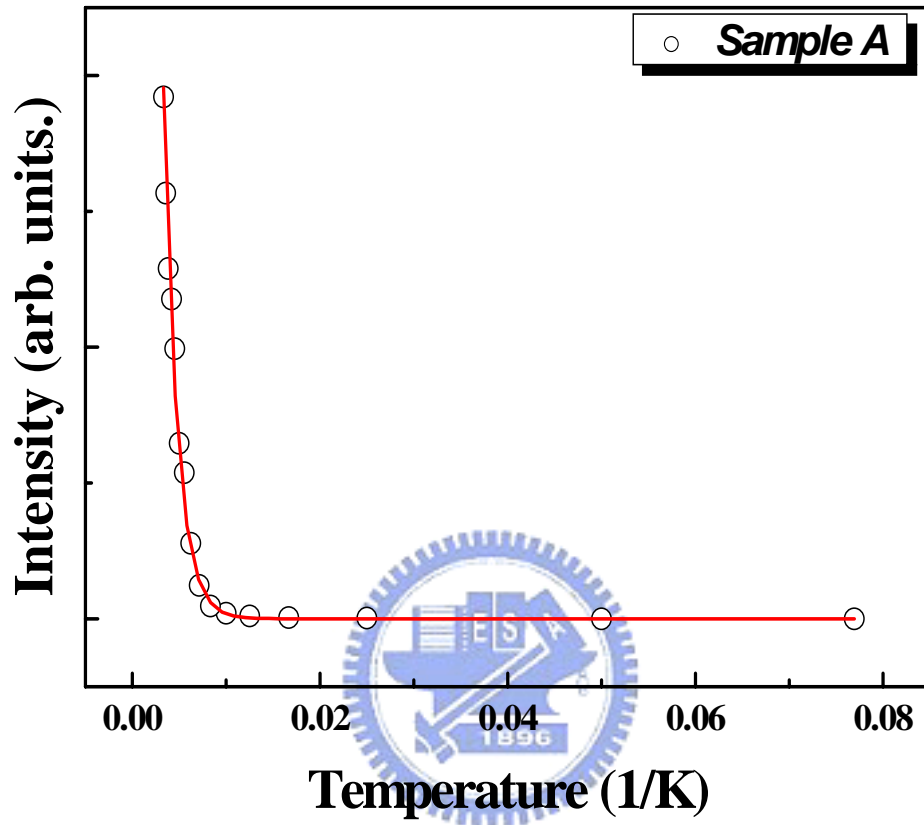


Fig. 3-6. Arrhenius plot of the integrated PL intensity, fitted by using Eq. (1) with sample A.

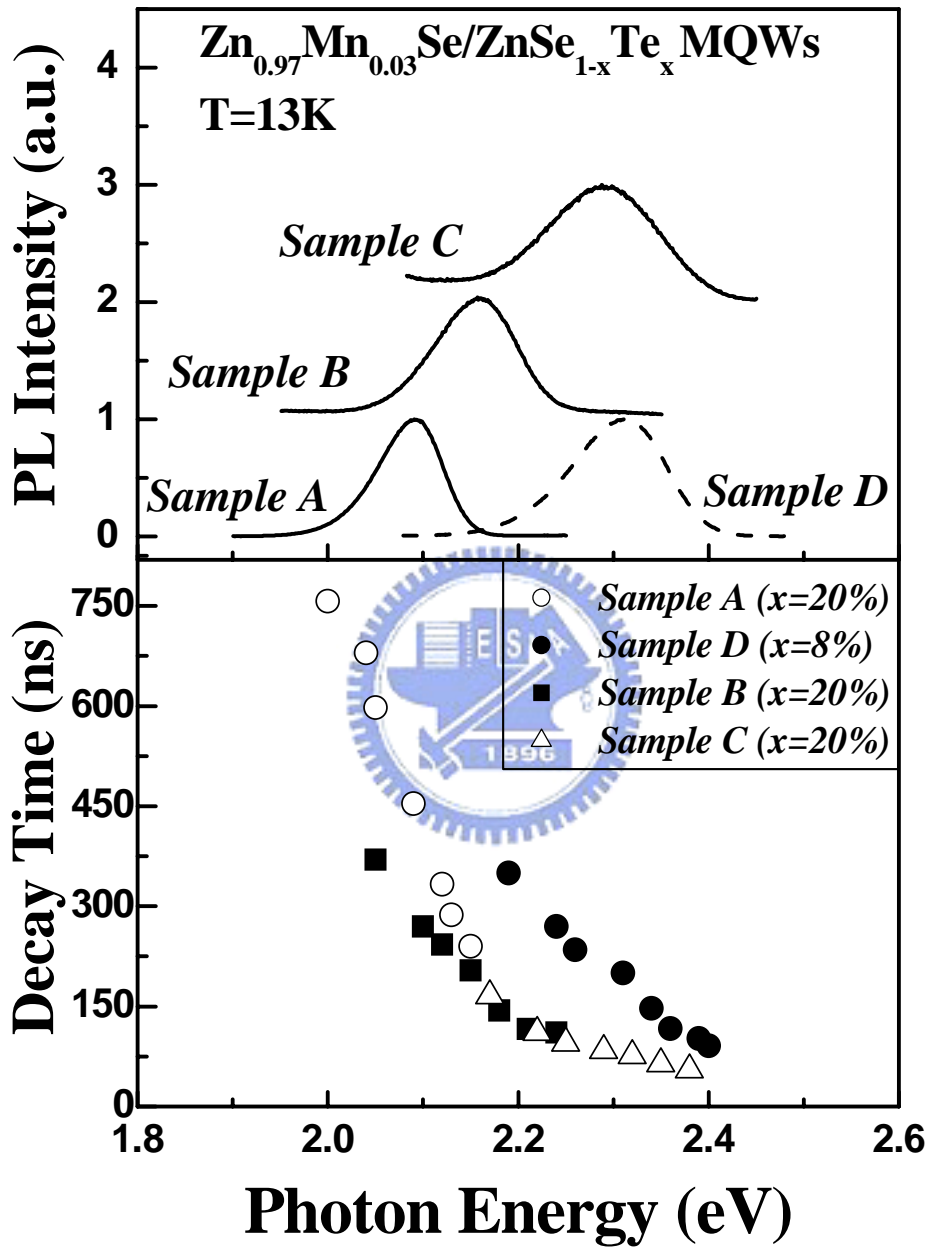


Fig. 3-7. The spectral distributions of the decay times for the Zn_{0.97}Mn_{0.03}Se/ZnSe_{1-x}Te_x (x=0.08 and 0.20) MQWs.

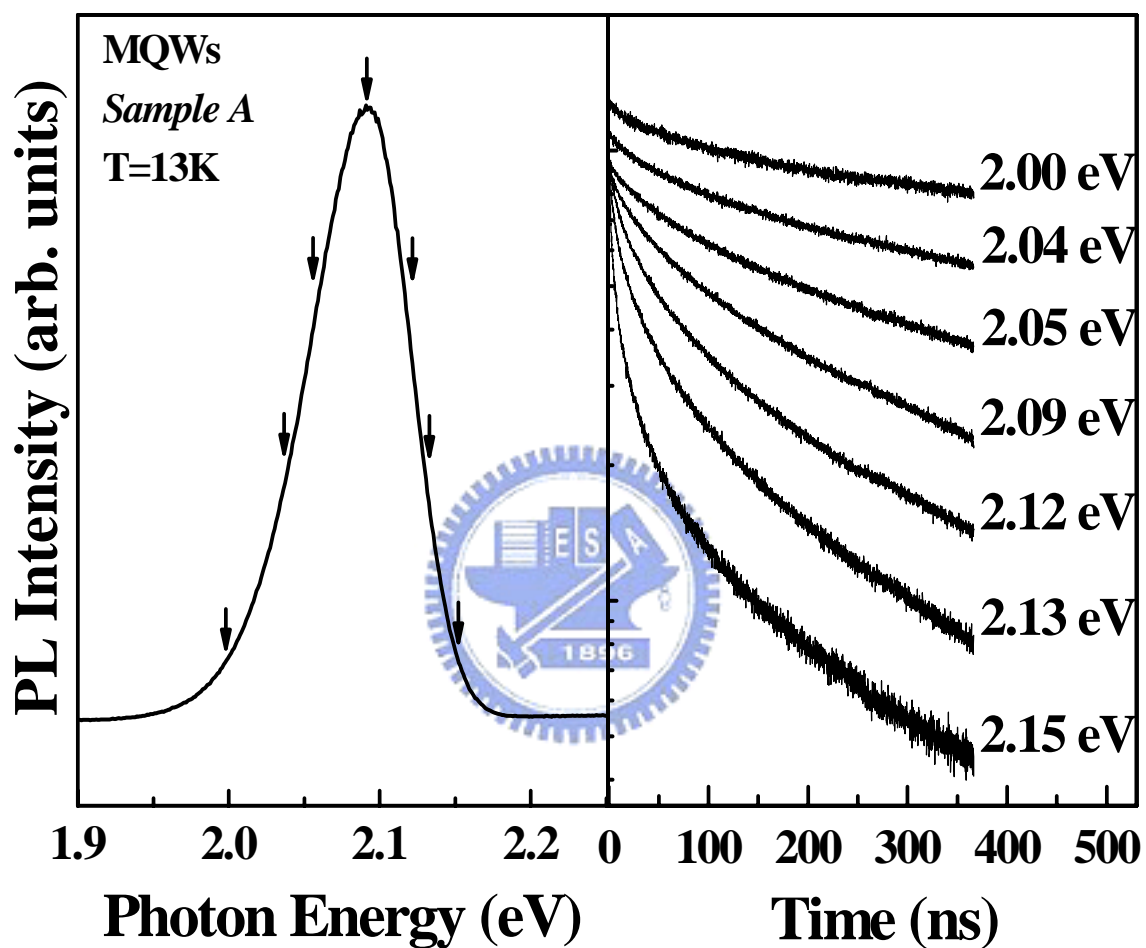
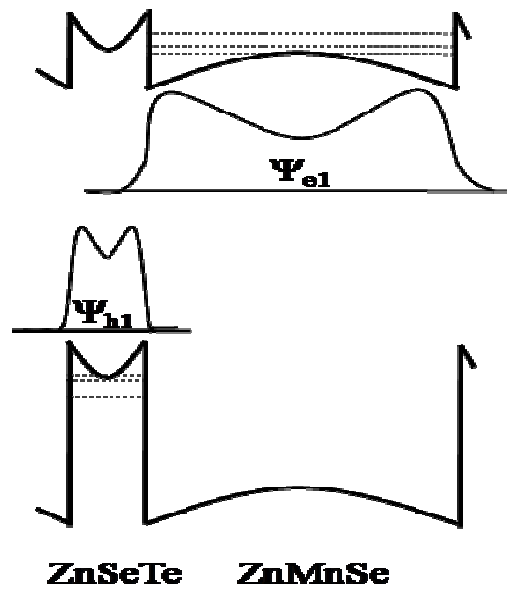
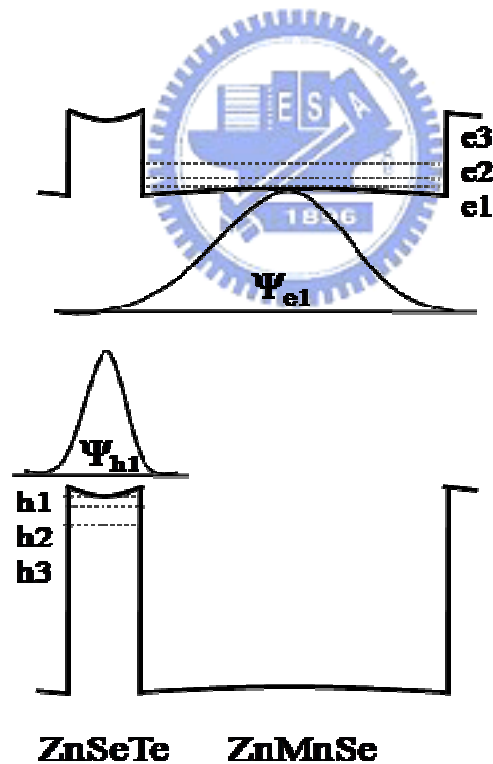


Fig. 3-8. (a) PL spectrum of sample A at 13 K.
(b) The spectral distribution of PL decay time of sample A at 13 K.



(a)



(b)

Fig. 3-9. Schematic representations for the electron and hole wave function distribution for (a) strong band-bending effect (b) weak band-bending effect.

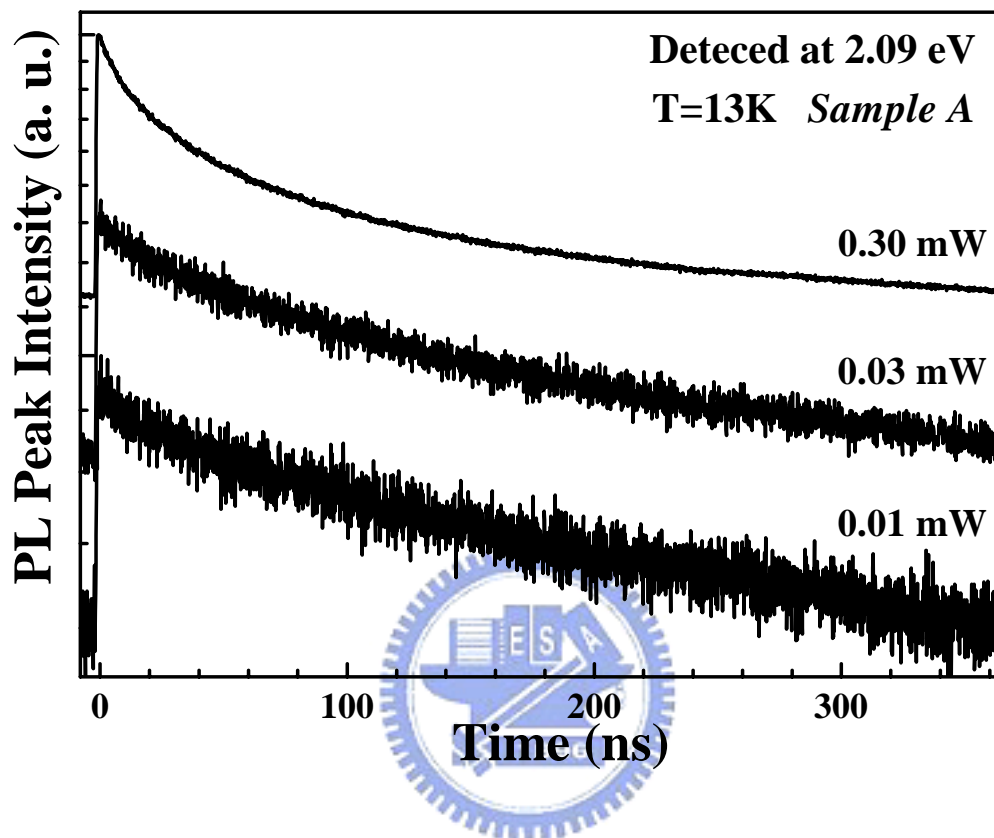


Fig. 3-10. The TRPL spectra of sample A recorded at different excitation intensities.

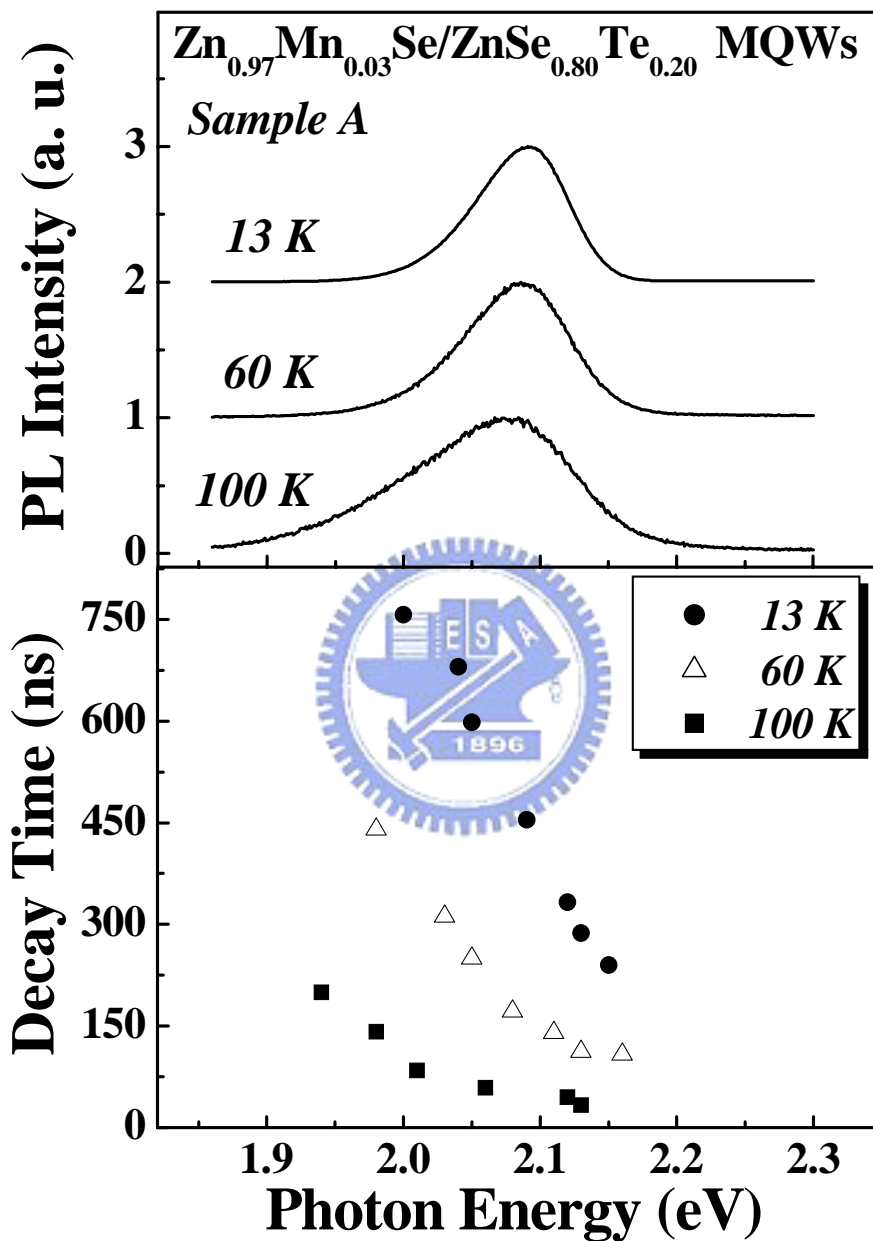


Fig. 3-11. The PL spectra and PL decay times of Zn_{0.97}Mn_{0.03}Se/ZnSe_{0.80}Te_{0.20} MQWs for sample A in different temperature.

Chapter 4 : Conclusions

In summary, we have studied the optical properties of $\text{Zn}_{0.97}\text{Mn}_{0.03}\text{Se}/\text{ZnSe}_{1-x}\text{Te}_x$ ($x = 0.08$ and 0.20) MQWs structures by using PL and TRPL measurements. The quantum confinement effect is confirmed by the energy shift of the PL peak energy. From excitation power-dependent PL, a type-II band alignment of the $\text{Zn}_{0.97}\text{Mn}_{0.03}\text{Se}/\text{ZnSe}_{1-x}\text{Te}_x$ MQWs is verified. The activation energies of the samples are about 46, 50 and 60 meV.

In addition, the long PL decay times from different well width and Te concentration is well-explained by wavefunction overlap. It indicates that the Te isoelectronic center plays an important role in the carrier recombination. The decay time is composed of a slower tail and a faster initial decay due to the band-bending effect. The results are supported by power-dependent TRPL measurements.

References

- [1] G. F. Neumark, R. M. Park, and J. M. Depuydt, *Phys. Today* **47**(6), 29 (1994)
- [2] D. B. Eason, Z. Yu, W. C. Hughes, W. H. Roland, C. Boney, J. W. Cook, Jr., J. F. Schetzina, G. Cantwell and W. C. Harsch, *Appl. Phys. Lett.* **66**, 115 (1995).
- [3] X. D. Luo, J. S. Huang, Z. Y. Xu, C. L. Yang, J. Liu, W. K. Ge, Y. Zhang, A. Mascarenhas, H. P. Xin, and C. W. Tu, *Appl. Phys. Lett.* **82**, 1697 (2003)
- [4] X. D. Yang, Z. Y. Xu, Z. Sun, Y. Ji, B. Q. Sun, I. K. Sou, and W. K. Ge, *Appl. Phys. Lett.* **86**, 162108 (2005)
- [5] M. C.-K. Cheung A. N. Cartwright, I. R. Sellers B. D. McCombe, and I.L. Kuskovsky, *Appl. Phys. Lett.* **92**, 032106 (2008)
- [6] Qiang Fu, D. Lee, A.V. Nurmiko, L. A. Kolodziejski, and R. L. Gunshor, *Phys. Rev. B* **39**, 3173 (1989)
- [7] C. S. Yang, D. Y. Hong, C. Y. Lin, W. C. Chou, C. S. Ro, W. Y. Uen, W. H. Lan, and S. L. Tu, *J. Appl. Phys.* **83**, 2555 (1998)
- [8] A. P. Jacob, Q. X. Zhao, M. Willander, C. S. Yang, and W. C. Chou, *J. Appl. Phys.* **94**, 2337 (2003)
- [9] S. P. Ahrenkiel, S. H. Xin, P. M. Reimer, J. J. Berry, H. Luo, M. Bode, M. Al-Jassim, J. R. Buschert, and J. K. Furdyna, *Phys. Rev. Lett.* **75**, 1586 (1995)

- [10] Jia Zhen Zheng, J. W. Allen, D. E. Spence, W. E. Sleat, and W. Sibbett, *Appl. Phys. Lett.* **62**, 63 (1992)
- [11] A. Reznitsky, S. Permogorov, S. Verbin, A. Naumov, Yu. Korostelin, V. Novozhilov, and S. Prokov'ev, *Solid State Comm.* **52**, 13 (1984)
- [12] K. Suzuki, U. Neukirch, J. Gutowski, N. Takojima, T. Sawada, and K. Imai, *J. Cryst. Growth* **184/185**, 882 (1998)
- [13] S. D. Baranovskii, U. Doerr, P. Thomas, A. Naumov, and W. Gebhardt, *Phys. Rev. B* **48**, 17149(1993)
- [14] M. J. Ludowise, D. Biswas and P. K. Bhattacharya, *Appl. Phys. Lett.* **56**, 958 (1990)
- [15] C. M. Lin, and Y. F. Chen, *Appl. Phys. Lett.* **85**, 2544 (2004)
- [16] N. N. Ledentsov, J. Bohrer, M. Beer, F. Heinrichsdorff, M. Grundmann, D. Bimberg, S. V. Ivanov, B. Ya. Meltser, S. V. Shaposhnikov, I. N. Yassievich, N. N. Faleev, P. S. Kop'ev, and Zh. I. Alferov, *Phys. Rev. B* **52**, 14058 (1995)
- [17] Y. S. Chiu, M. H. Ya, W. S. Su, and Y. F. Chen, *J. Appl. Phys.* **92**, 5810 (2002)
- [18] E. Tournie', C. Morhain, M. Leroux, C. Ongaretto, and J. P. Faurie, *Appl. Phys. Lett.* **68**, 1543 (1996)
- [19] J. T. Ku, M. C. Kuo, J. L. Shen, K. C. Chiu, T. H. Yang, G. L. Luo, C. Y. Chang, Y. C. Lin, C. P. Fu, D. S. Chuu, and W. C. Chou *J. Appl. Phys.* **99**, 063506 (2006)

- [20] C.-K. Sun, G. Wang, J. E. Bowers, B. Brar, H.-R. Blank, H. Kroemer, and M. H. Pilkuhn, *Appl. Phys. Lett.* **68**, 1543 (1996)
- [21] Y. Gu, Igor L. Kuskovsky, M. van der Voort, G. F. Neumark, X. Zhou, and M. C. Tamargo, *Phys. Rev. B* **71**, 045340 (2005)

